Acta Med. Okayama, 2025
Vol. 79, No. 1, pp. 21–30

Acta Medica Okayama
http://escholarship.lib.okayama-u.ac.jp/amo/

Original Article

Prediction of Prostate Cancer Grades Using Radiomic Features

Yasuhiro Yamamoto[a]*, Takafumi Haraguchi[b], Kaori Matsuda[a], Yoshio Okazaki[a], Shin Kimoto[a], Nozomu Tanji[c], Atsushi Matsumoto[c], Yasuyuki Kobayashi[d], Hidefumi Mimura[e], and Takao Hiraki[f]

Departments of [a]Radiology, [c]Urology, Houshasen Daiichi Hospital, Imabari, Ehime 794-0054, Japan,
Departments of [b]Advanced Biomedical Imaging and Informatics, [d]Medical Information and Communication Technology Research,
[e]Radiology, St. Marianna University School of Medicine, Kawasaki, Kanagawa 216-8511, Japan,
[f]Department of Radiology, Okayama University Graduate School of Medicine, Dentistry and Pharmaceutical Sciences, Okayama 700-8558, Japan

We developed a machine learning model for predicting prostate cancer (PCa) grades using radiomic features of magnetic resonance imaging. 112 patients diagnosed with PCa based on prostate biopsy between January 2014 and December 2021 were evaluated. Logistic regression was used to construct two prediction models, one using radiomic features and prostate-specific antigen (PSA) values (Radiomics model) and the other Prostate Imaging-Reporting and Data System (PI-RADS) scores and PSA values (PI-RADS model), to differentiate high-grade (Gleason score [GS] ≥ 8) from intermediate or low-grade (GS < 8) PCa. Five imaging features were selected for the Radiomics model using the Gini coefficient. Model performance was evaluated using AUC, sensitivity, and specificity. The models were compared by leave-one-out cross-validation with Ridge regularization. Furthermore, the Radiomics model was evaluated using the holdout method and represented by a nomogram. The AUC of the Radiomics and PI-RADS models differed significantly (0.799, 95% CI: 0.712-0.869; and 0.710, 95% CI: 0.617-0.792, respectively). Using holdout method, the Radiomics model yielded AUC of 0.778 (95% CI: 0.552-0.925), sensitivity of 0.769, and specificity of 0.778. It outperformed the PI-RADS model and could be useful in predicting PCa grades, potentially aiding in determining appropriate treatment approaches in PCa patients.

Key words: prostate cancer, machine learning, prostate Imaging-Reporting and Data System, radiomics, Gleason score

Prostate cancer (PCa) is known to be highly prevalent among individuals of European and American descent. However, in recent years, the number of patients with PCa has demonstrated a sharp increase in Japan [1]. PCa is the second most common cancer in men, with 1,276,106 new cases and 358,989 deaths reported worldwide in 2018 [2]. The incidence of PCa increases with age, with men aged 50 years and older at a higher risk.

Prostate-specific antigen (PSA) is a protein produced by the prostate gland, which is typically present in the prostate tissue. Elevated blood PSA levels may indicate PCa or other prostate-related conditions. PSA testing plays a crucial role in the early detection of PCa, and periodic PSA screenings are commonly used as a general screening method for PCa. However, PSA test results are used in combination with other factors to

Received May 7, 2024; accepted October 8, 2024.
*Corresponding author. Phone: +81-898-23-3358; Fax: +81-898-23-8868
E-mail: tw_blitzen@yahoo.co.jp (Y. Yamamoto)

Conflict of Interest Disclosures: No potential conflict of interest relevant to this article was reported.

assess the risk of PCa, as elevated PSA levels do not always indicate PCa and can result from conditions such as inflammation or benign prostatic hyperplasia (BPH).

The Gleason score (GS) is one of the most important predictors of PCa prognosis. The GS is used to grade the aggressiveness of PCa based on the microscopic appearance of the tumor tissue. It provides valuable information regarding the appearance of abnormal or aggressive cancer cells under a microscope. The GS helps in assessing prognosis and guiding treatment decisions in individuals with PCa.

Patients can be categorized into GS ≤7 (low-grade PCa) and GS >7 (high-grade PCa), and high-grade PCa accounts for approximately 15% of all patients with PCa [3]. A study has shown that the 5-year recurrence-free progression probabilities for low-grade PCa (63-96%) and high-grade PCa (26-48%) are significantly different [4].

Patients with low-grade PCa may benefit from relatively conservative treatment strategies or short-term neoadjuvant antiandrogen therapy (ADT) for 4-6 months, while patients with high-grade PCa are recommended to undergo longer ADT (2-3 years), which may improve their prognosis and reduce mortality [5-7]. However, the GS can only be determined via needle biopsy or resection [8-10]. The complications of prostate biopsy include bleeding, infection, and urinary issues, and older individuals and those with underlying health conditions may have an increased risk of biopsy-related complications. Therefore, the accurate noninvasive identification of high-grade PCa at the initial diagnosis or before surgery is very important in order to optimize treatment decision-making and improve the prognosis in this patient population.

Machine learning is a field of artificial intelligence (AI) covering an extensive range of algorithms that can be trained to perform certain tasks, such as classification. Supervised learning methods, which use labeled data to guide the algorithm, have arguably shown the greatest success in medical imaging, with applications in the diagnosis of metastatic disease, diabetic retinopathy, and intracranial hemorrhage [11, 12].

Radiomic analysis is defined as the computational extraction of quantitative image features for the characterization of disease patterns. The analyzed image features include shape features, first-order statistics, and texture characteristics, such as gray-level co-occurrence matrices (GLCMs) [13]. Recent advances in image analysis techniques using radiomic features to assess the genomic, proteomic, and clinical phenotypes of prostate tumors have been shown to match or even surpass the qualitative imaging assessment of radiologists [14-16].

Bagher-Ebadian *et al.* reported that a radiomics model could differentiate PCa lesions from normal prostate tissues with an area under the curve (AUC), positive predictive value (PPV), and negative predictive value (NPV) of 0.94, 0.95, and 0.92, respectively [17]. Chaddad *et al.* found a significant correlation between GLCM features extracted jointly from T2-weighted images (T2WIs) and apparent diffusion coefficient (ADC) images and GS, with an AUC of 0.78 for GS ≤3, 0.82 for GS 3+4, and 0.65 for GS ≥4+3 [18]. Monti *et al.* found that standard radiomics models using T2WIs and ADC images performed better for PCa detection than did an advanced model with additional diffusion kurtosis imaging and dynamic contrast-enhanced (DCE) magnetic resonance imaging (MRI) [19]. However, to the best of our knowledge, no model combining clinical PSA values with information obtained from imaging, such as Prostate Imaging-Reporting and Data System (PI-RADS) scores or radiomics features, has yet been sufficiently investigated.

In this study, we developed a machine learning model based on radiomic features of MRI before prostate biopsy and the PSA value and evaluated its diagnostic performance. Additionally, we compared the performance of the model with PI-RADS scores for predicting high-grade PCa (GS ≥8).

Materials and Methods

This study focused on 160 consecutive cases of PCa diagnosed based on prostate biopsies at our institution between January 2014 and December 2021. Of these, 48 cases were excluded because the grade of the PCa lesions could not be identified using MRI, or due to poor image quality and repeat biopsy. Ultimately, a total of 112 patients were selected for the study.

The study protocol for MRI examination and prostate biopsy in patients with PCa was approved by the Ethical Committee of Housyasen Daiichi Hospital (Approval No. 02). Due to the retrospective nature of the study, acquisition of informed consent was waived. All procedures were performed in accordance with the

relevant guidelines and regulations of the Declaration of Helsinki.

The age of the patients ranged from 52 to 93 years (mean age: 73.6 ± 7.8 years). The biopsy procedure involved the insertion of an ultrasound device through the anus into the rectum. While observing the prostate through the rectal wall using ultrasound, a biopsy needle was inserted through the rectal wall into the prostate. Tissue samples were collected from four locations on each side. The pathological GSs were distributed as follows: GS 6 in 16 cases, GS 7 in 29 cases, GS 8 in 20 cases, GS 9 in 38 cases, and GS 10 in 9 cases. A total of 80 patients showed lesions in the peripheral zone only, 27 had lesions in the transition zone only, and 5 had lesions in both the peripheral and transition zones.

GSs were determined and standardized by two pathologists. In cases in which their initial assessments did not match, detailed discussions were held to review and reconcile the differences to establish a final score. The PSA levels of the 112 individuals ranged from 2.31 to 966.09 ng/ml (34.93 ± 9.71).

The Philips Ingenia 1.5-T system was used for MRI. For radiomics analysis, ADC images generated from diffusion-weighted imaging (DWI) with *b*-values of 0 and 2,000, and T2WI were used.

The imaging parameters for MRI are listed in Table 1.

PI-RADS score. In each patient, one representative lesion was selected from the MRI images, and a PI-RADS score was assigned by consensus by two radiologists, each with at least 10 years of radiology experience. The scoring was based on PI-RADS version 2.1 [20]. Since contrast-enhanced MRI was not conducted, a lesion in the peripheral zone that was assigned a score of 3 on DWI was evaluated as PI-RADS score 3.

Table 1 MRI parameters of the study

	T2WI	DWI $b=0$, 2,000
FOV	320 × 320	320 × 320
Matrix	412	104
Technique	SE	SE
Fast Imaging	TSE-multi shot	EPI-single shot
Recon-pixel size	0.50 × 0.50	2.00 × 2.00
SENSE	1.3	2
Slices	24	24
Slices-thickness	3	3
Gap	0.3	0.3
Profile order	Linear	–
BW	269.7	25.9
Factor	16	67
TE	90	80
TR	4,000	6,250
Fat suppression	–	SPAIR
NSA	1	4

T2WI, T2-weighted images; DWI, Diffusion weighted imaging.

Regions of interest (ROIs) setting. Research annotation software (Canon Medical Systems, Otawara, Japan) was used to segment representative tumor lesions in the MRI images (T2WI and ADC images). The first radiologist delineated an ROI for each case. To assess reproducibility, a second radiologist randomly selected ROIs from 20 cases for verification.

Radiomic features. An open-source package (PyRadiomics ver. 3.0.1) was used to extract 107 radiomic features.

Radiomic features were extracted from 20 randomly selected nodules, each segmented by two radiologists (each with > 10 years of experience).

Only features demonstrating high interobserver and intraobserver reliability (intraclass correlation coefficient [ICC] > 0.75) were chosen. Five radiomic features were then selected based on their importance, as determined by the Gini coefficient, and these features, along with PSA values, were used as the explanatory variables.

Model development. A classification prediction was performed in the high-grade (GS ≥ 8) and intermediate/low-grade (GS < 8) PCa groups. Two models were developed: a Radiomics model based on radiomic features and PSA values, and a PI-RADS model utilizing the PI-RADS scores and PSA values as the explanatory variables. Orange3 (ver. 3.32.0) was used for development [21]. These two models were evaluated using the leave-one-out and holdout methods. In addition, the AUC values for the PSA-only, radiomics-only, and PI-RADS-only models were calculated using the leave-one-out method.

1. Leave-one-out method. Both models were constructed using logistic regression (Fig. 1). In each loop, the features were standardized and 9 features were selected using the Gini index, which was calculated from two cumulative relative frequencies: one for radiomics features and the other for the proportion of high-grade PCa. Receiver operating characteristic (ROC) curves were plotted; the predictive accuracy was evaluated using the leave-one-out method.

2. Holdout method. Next, a logistic regression

model was created using radiomics features and PSA values, followed by model construction and the evaluation of accuracy using the holdout method. Twenty percent of the total data were randomly extracted as the test data and the remaining 80% were used as the training data (Fig. 2). The training data were standardized and the same standardization was applied to the test data. Five features were selected using the Gini index, which was calculated as described above. The importance of the explanatory variables was computed from the predictive model, and a nomogram was constructed.

Statistical analysis. Statistical analysis was conducted using R software (version 4.2.1; http://www.r-project.org). The AUC values were measured and the sensitivity, specificity, PPV, and NPV were calculated based on the Youden index. The AUC values of the two models were compared using the DeLong test and the leave-one-out method. Statistical significance was set at $p < 0.05$.

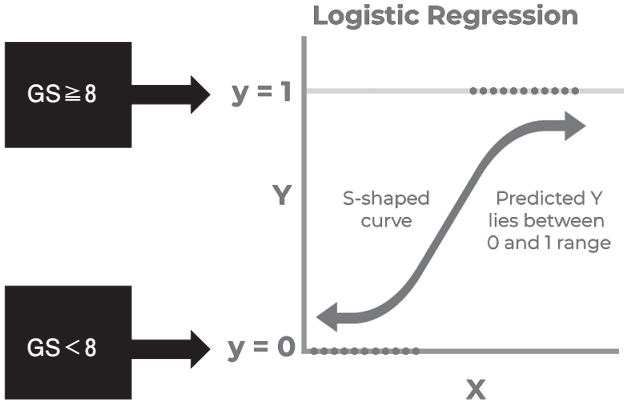

Fig. 1 Logistic regression model. A logistic regression model for predicting high- and low-grade prostate cancer (PCa) was developed and validated using the leave-one-out cross-validation method.

Results

Leave-one-out method. Figure 3 shows the ROC curves for the radiomic features and PSA value-based model (Radiomics model) and for the PI-RADS score and PSA value-based model (PI-RADS model). The Radiomics model yielded the following results: AUC, 0.799; sensitivity, 55.8%; specificity, 88.9%; PPV, 88.2%; and NPV, 57.5%. The PI-RADS model showed the following results: AUC, 0.710; sensitivity, 71.6%; specificity, 71.1%; PPV, 82.3%; and NPV, 62.7%. Thus, the Radiomics model demonstrated significantly higher AUC and PPV values than the PI-RADS model ($p < 0.05$).

The AUC values for the PI-RADS-only, Radiomics-only, and PSA-only models were 0.590, 0.778, and 0.752, respectively.

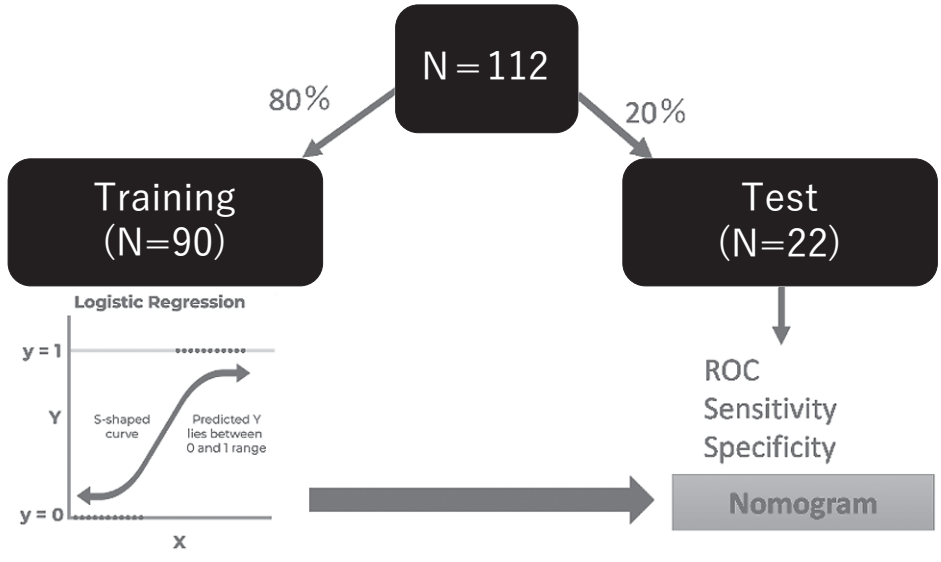

Fig. 2 Holdout method. A logistic regression model was developed and evaluated using the holdout method. Using the Gini coefficient, five explanatory variables were selected from among the radiomic features and standardized. A nomogram was created using the selected features and prostate-specific antigen (PSA) values.

The analysis results for the GS, PSA, PI-RADS, and radiomics are presented in Table 2. Considering PI-RADS scores of 4 or higher as positive, the sensitivity and specificity of the PI-RADS group were 88.1% and 37.8%, respectively. In the radiomics group, the sensitivity and specificity were 76.1% and 62.2%, respectively.

Holdout method. Next, the data were divided into training and test sets, and a model was constructed using the training data. The Radiomics model was analyzed using logistic regression. When applied to the test data, the model demonstrated high accuracy, with an AUC of 0.778, sensitivity of 0.769, and specificity of 0.778. The results of the Gini index are presented in Table 3.

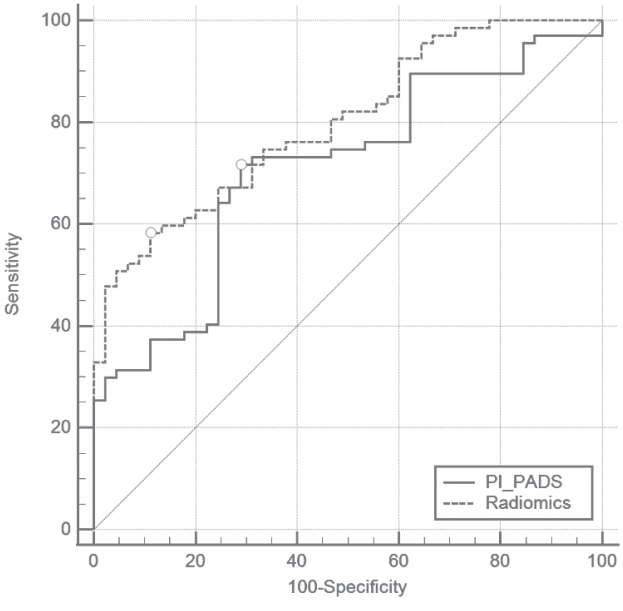

Fig. 3 Receiver operating characteristic (ROC) curves of the two models using the leave-one-out method.

The contributions of the selected radiomic features and the PSA value were determined. The results are displayed along with brief definitions of each radiomic feature. The PSA value indicated a contribution of 0.929. The shape feature Maximum 2D Diameter

Table 3 The results of the Gini index

Radiomic feature	Gini Index
PSA	0.1085
PI-RADS	0.0924
Major Axis Length ADC	0.0934
Max 2D Diameter Column ADC	0.088
Max 2D Diameter Row ADC	0.0753
Max 2D Diameter Slice ADC	0.0934
Max 3D Diameter ADC	0.0934
Mesh Volume ADC	0.107
Minor Axis Length ADC	0.0806
Sphericity ADC	0.0915
Surface Area ADC	0.112
Voxel Volume ADC	0.1024
First-order Entropy ADC	0.0499
First-order Uniformity ADC	0.0493
GLCM Joint Energy ADC	0.0456
GLCM Maximum Probability ADC	0.0413
GLCM Sum of Squares ADC	0.0284
GLDM Dependence Variance ADC	0.0312
GLDM Gray Level Variance ADC	0.0499
GLDM Large Dependence Low Gray Level Emphasis ADC	0.0682
GLRLM Long Run Low Gray Level Emphasis ADC	0.0755
GLRLM Run Variance ADC	0.0755
NGTDM Contrast ADC	0.0706
Max 2D Diameter Column T2WI	0.133
Minor Axis Length T2WI	0.1069
Surface Volume Ratio T2WI	0.0551
First-order 10th Percentile T2WI	0.0458
GLRLM Gray Level Non-Uniformity T2WI	0.0927
GLRLM Run Entropy T2WI	0.1211
GLSZM Zone Percentage T2WI	0.1212

ADC, apparent diffusion coefficient; GLCM, gray level co-occurrence matrices; GLDM, gray-level dependence matrix; GLRLM, gray level run-length matrix; GLSZM, gray level size zone matrix; PSA, prostate-specific antigen; PI-RADS, Prostate Imaging-Reporting and Data System; T2WI, T2-weighted images.

Table 2 The analysis results for the GS, PSA, PI-RADS (P), and radiomics (R)

GS	P (+), R (+)	P (+), R (−)	P (−), R (+)	P (−), R (−)	PSA	total
6	4	6	1	5	2.31–51.67	16
7	9	9	3	8	4.70–17.32	29
8	11	5	1	3	3.43–488.69	20
9	30	5	0	3	4.70–966.09	38
10	8	0	1	0	7.06–322.44	9

GS, Gleason score; PI-RADS, Prostate Imaging-Reporting and Data System; PSA, prostate-specific antigen.

Column from T2WI, which represents the largest diameter of the lesion in the 2D plane, had a contribution of 0.905. The gray level size zone matrix (GLSZM) feature Zone Percentage from T2WI, indicating the percentage of homogeneous zones in the GLSZM, showed a contribution of −0.565. The gray level run length matrix (GLRLM) feature Run Entropy from T2WI, representing the entropy of runs in the GLRLM, had a contribution of 0.205. Finally, the shape feature Surface Area from ADC imaging, denoting the surface area of the lesion, showed a contribution of 0.0788. The larger the absolute value, the greater the degree of contribution.

Of the 67 cases of GS ≥ 8, 6 could not be identified correctly by either the PI-RADS model or the Radiomics model. Although 10 patients had a PI-RADS score of 4 or 5, they were not diagnosed with high-grade PCa by the radiomics approach. In contrast, the PI-RADS score 2 and score 3 groups included 8 cases of GS ≥ 8. Of these, 2 were correctly diagnosed with high-grade PCa using the radiomics approach. The cases that were incorrectly classified by the Radiomics and PI-RADS models are presented in Figs. 4 and 5, respectively. In 19 cases, both PI-RADS and Radiomics were negative, and 6 of these cases had GS ≥ 8.

Nomogram. Finally, we created a nomogram for predicting high-grade (GS ≥ 8) PCa using the selected radiomic features (Fig. 6). The values were standardized as Z = (X − mean)/standard deviation.

Discussion

Preoperative prediction of the PCa grade is important for clinical decision-making. Pathological biopsy is a popular tool for estimating the PCa grade and invasiveness; however, it is associated with several compli-

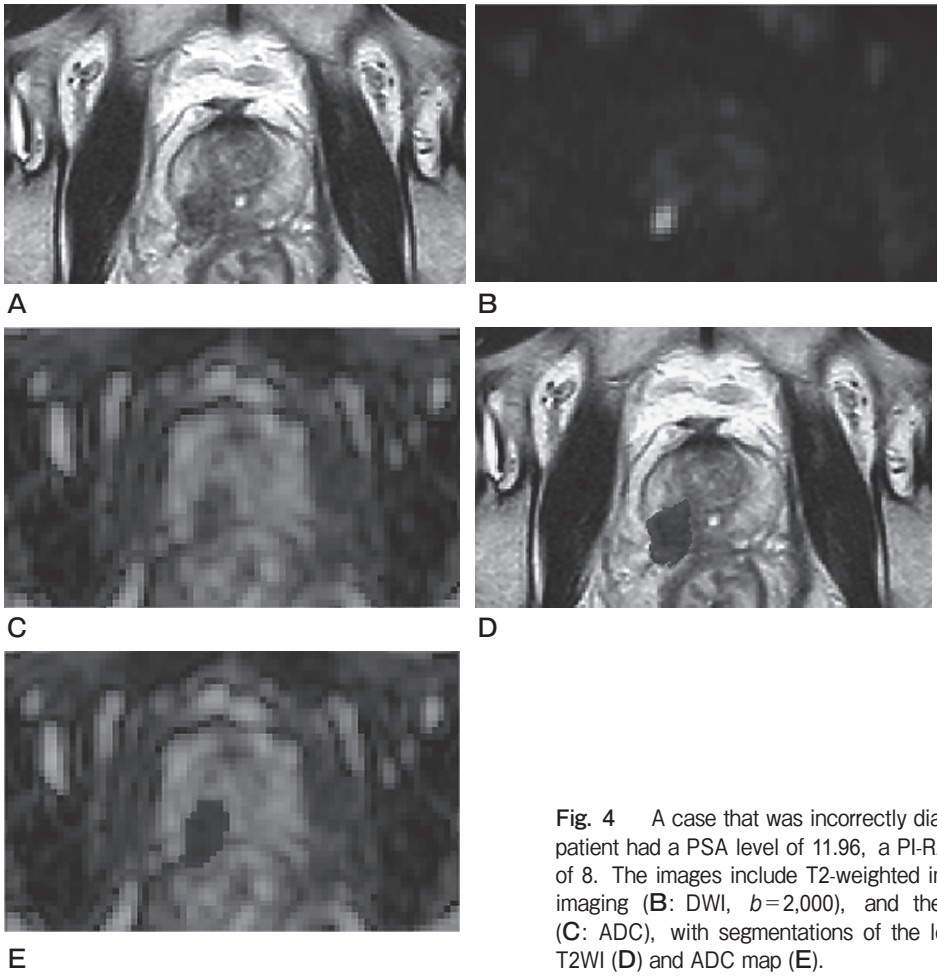

Fig. 4 A case that was incorrectly diagnosed by the Radiomics model. The patient had a PSA level of 11.96, a PI-RADS score of 5, and a Gleason score of 8. The images include T2-weighted imaging (**A**: T2WI), diffusion-weighted imaging (**B**: DWI, $b = 2{,}000$), and the apparent diffusion coefficient map (**C**: ADC), with segmentations of the lesion highlighted in dark gray on the T2WI (**D**) and ADC map (**E**).

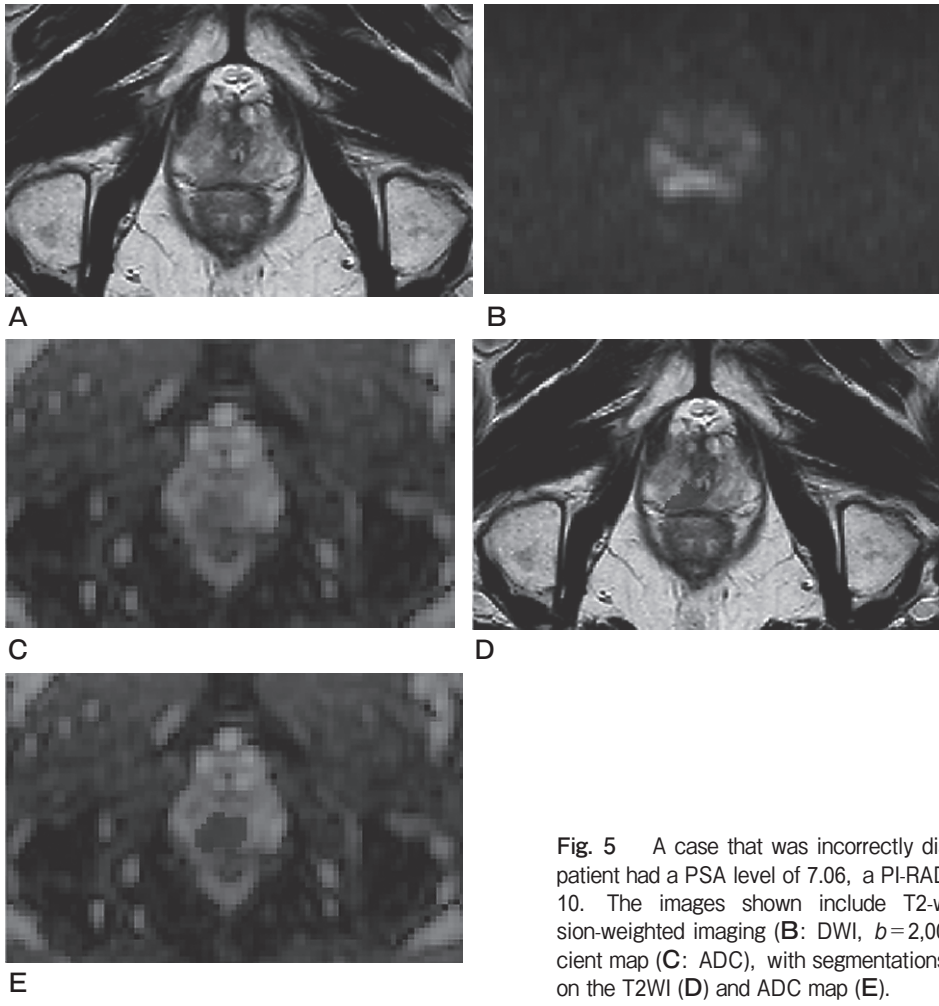

Fig. 5 A case that was incorrectly diagnosed by the PI-RADS model. The patient had a PSA level of 7.06, a PI-RADS score of 3, and a Gleason score of 10. The images shown include T2-weighted imaging (**A**: T2WI), diffusion-weighted imaging (**B**: DWI, $b=2{,}000$), and the apparent diffusion coefficient map (**C**: ADC), with segmentations of the lesion highlighted in dark gray on the T2WI (**D**) and ADC map (**E**).

cations that limit its clinical use.

In this study, we developed a radiomics and PSA-based machine learning model for predicting high-grade PCa and compared its diagnostic efficacy with that of PI-RADS v2.1 scores. PI-RADS is a diagnostic method that expresses the confidence level of clinically significant PCa (GS ≥ 7) in five categories.

PCa is curable if it remains confined to the prostate, after which it is classified into low-risk, intermediate-risk, and high-risk localized and locally advanced PCa. These risk classes form the basis for treatment. Low-risk PCa is treated with "active surveillance," and the prognosis is excellent. In patients with low-intermediate risk, active surveillance should also be discussed as an option. In other cases, active treatments such as surgery or radiation therapy should be discussed along with their potential side effects to allow for shared decision-making [22]. The present study evaluates a model for detecting high-risk PCa with GS ≥ 8. However, there are no particular issues resulting from using PI-RADS as the diagnostic method.

Radiomics features were extracted and selected from T2WI and ADC images; these features along with the PSA values were used to construct a model based on logistic regression. In general, T2WI and ADC are the most common sequences selected by investigators for texture analysis [23, 24]. Additionally, the PI-RADS v2.1 scoring system increases the diagnostic weight of T2WI and ADC images and reduces the diagnostic weight of DCE images [25]. Therefore, we chose to derive radiomics features from only T2WI and ADC images in the present study.

In our study, the Radiomics model showed a higher AUC for predicting high-grade PCa (GS ≥ 8) than the

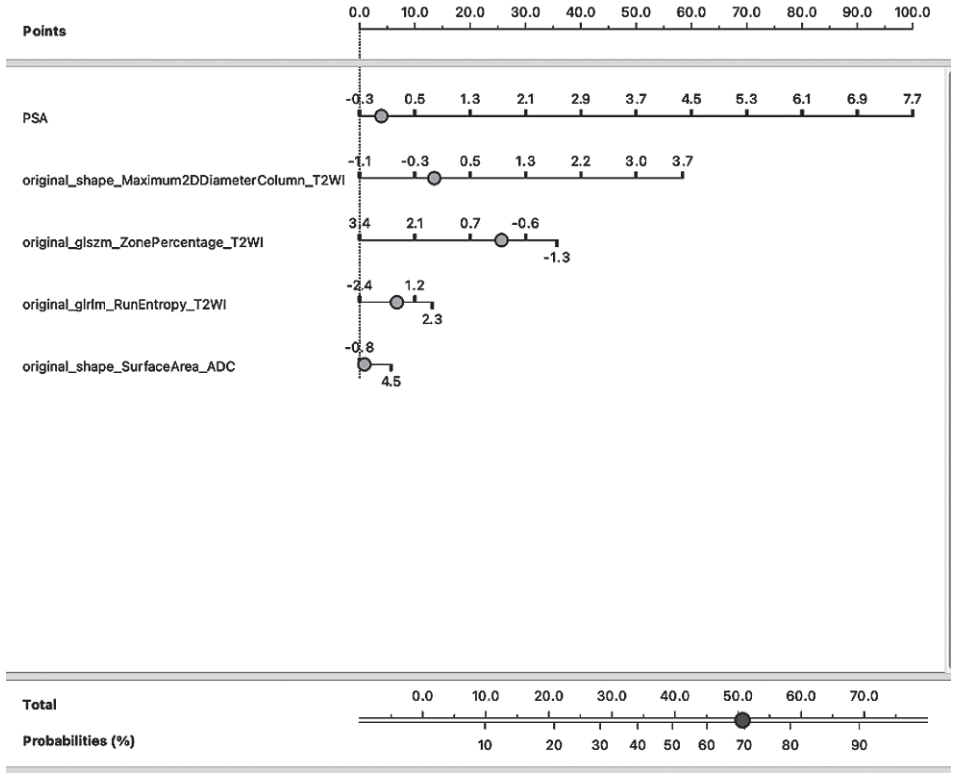

Fig. 6 Nomogram.

PI-RADS model (AUC: 0.799 vs. 0.710; $p<0.05$). Chen *et al.* report that a radiomics-based model with T2WI and ADC features outperformed the PI-RADS score in assessing PCa differentiation [26]. We used a model that includes the PSA value; similar to the findings by Chen *et al.*, radiomics features were found to be more effective than PI-RADS values for predicting high-grade PCa. The effectiveness of radiomics features suggests that the long diameter and volume of the tumor could be crucial for predicting high-grade PCa, with larger values indicating higher malignancy, consistent with the results of previous studies. The intracellular components, internal fluid volume, collagen volume, and myofibrous stroma differ between the different pathologic grades of PCa. High-grade PCa has a high cell count and reduced extracellular space, while low-grade PCa retains at least some glandular structures and intercellular space [27, 28]. These differences in the histopathological features may be reflected by quantitative analyses using the radiomics approach.

Among the 67 cases of GS ≥ 8, 6 could not be accurately identified by either the PI-RADS model or the Radiomics model. Ten patients tested positive using PI-RADS but were judged negative using radiomics. Conversely, the group that tested negative using PI-RADS included 8 cases of a GS of 8 or higher, of which 2 were judged positive based on radiomics. These findings indicate that the two models may have complementary roles.

Furthermore, the AUC values for the PI-RADS-only, Radiomics-only, and PSA-only models were 0.590, 0.778, and 0.752, respectively. Based on the results shown in Table 4, the PI-RADS model exhibited very high sensitivity, but low specificity compared to the Radiomics model. The high sensitivity of PI-RADS is effective in detecting lesions (preventing missed diagnoses), while the high specificity of Radiomics is useful for avoiding false positives. In this study, both PI-RADS and Radiomics showed negativity in 19 cases, 6 of which had GS ≥ 8. If these cases were excluded from biopsy, 17% of biopsies could have been avoided. However, 9% of high-grade PCa would have been missed.

The interpretation of PI-RADS scores from MRI

images in the diagnosis of PCa is subjective and highly reader-dependent, while the machine learning model is quantitative and relatively objective, and demonstrates better diagnostic performance with radiomic features than do PI-RADS scores. This suggests that the radiomics approach is a promising technique for optimizing existing routine work.

Cases misclassified using the Radiomics and the PI-RADS models are shown in Figs. 4 and 5, respectively. In Fig. 4, an extracapsular extension of the tumor is evident, resulting in a high PI-RADS score. However, since radiomics cannot perform anatomical evaluation, there is a possibility that it may be evaluated as a low-grade malignancy. In Fig. 5, since there was no prominent low-signal intensity on the ADC map, the PI-RADS score was low at 3. However, if contrast-enhanced MRI was performed and enhancement was observed, the score could have been 4, potentially providing a more accurate prediction.

Chen *et al.* reported no significant differences in the diagnostic performance for PCa between Radiomics models using biparametric (bp) MRI (T2WI + DWI) and multiparametric (mp) MRI (T2WI + DWI + DCE) [29]. Zhang *et al.* showed that machine learning-based analysis based on a bp MRI radiomic model may be helpful in distinguishing between high- and low-grade PCa, and this analysis it outperformed the PI-RADS v2.1 scores based on mp MRI [30].

The present study utilized bp MRI, which was found to have sufficient prediction accuracy. Bagher-Ebadian *et al.* identified and ranked discriminant radiomic features from T2WI and ADC maps and constructed an adaptive model for characterizing significant intraprostatic lesions (DILs) and normal prostatic gland tissues (NT) [31].

Recently, there has been an increase in the availability of tools that can easily extract and analyze radiomic features in clinical settings [32]. The present results demonstrate that, with the combination of PSA values and the construction of nomograms, there exists the potential for the straightforward application of radiomics in clinical practice.

Limitations. Our study has certain limitations. First, all pathological results were derived from biopsy and lacked further validation with radical prostatectomy specimens. Histological-radiological matching was performed by experienced radiologists based on the biopsy site and MRI, which is an inevitable source of bias. Second, our study did not distinguish between peripheral and transitional PCa because PCa was observed in both zones in some cases. PI-RADS is a diagnostic method that expresses the confidence level of clinically significant PCa (GS $\geq$7) in five categories. However, our study evaluated a model for detecting PCa with GS $\geq$8. Additionally, in several cases, lesions were difficult to identify on MRI or regenerative disease was present; these cases were excluded from the study, which may have introduced a selection bias. Future studies should include larger study populations and evaluate peripheral and transitional PCa separately. Additionally, although our study extracted partial data to validate the radiomics-based model, external validation cohorts should also be used in future studies to test the reproducibility of the results.

In this study, a machine learning model based on radiomics features of PCa and PSA values obtained from MRI images was shown to successfully predict high-grade PCa (GS $\geq$8). This approach may assist in determining the appropriate treatment for patients with PCa.

Acknowledgments. The authors gratefully acknowledge the technical assistance of Kenji Kamida, Sumiko Ochi, Kazuyuki Sogabe and the other members of the Department of Radiological Technology, Houshasen Daiichi Hospital.

References

1. Taitt HE: Global Trends and Prostate Cancer: A Review of Incidence, Detection, and Mortality as Influenced by Race, Ethnicity, and Geographic Location. Am J Mens Health (2018) 12: 1807–1823.
2. Rawla P: Epidemiology of Prostate Cancer. World J Oncol (2019) 10: 63–89.
3. Gong L, Xu M, Fang M, Zou J, Yang S, Yu X, Xu D, Zhou L, Li H, He B, Wang Y, Fang X, Dong D and Tian J: Noninvasive Prediction of High-Grade Prostate Cancer via Biparametric MRI Radiomics. J Magn Reson Imaging (2020) 52: 1102–1109.
4. Epstein JI, Zelefsky MJ, Sjoberg DD, Nelson JB, Egevad L, Magi-Galluzzi C, Vickers AJ, Parwani AV, Reuter VE, Fine SW, Eastham JA, Wiklund P, Han M, Reddy CA, Ciezki JP, Nyberg T and Klein EA: A Contemporary Prostate Cancer Grading System: A Validated Alternative to the Gleason Score. Eur Urol (2016) 69: 428–435.
5. Carroll PH and Mohler JL: NCCN Guidelines Updates: Prostate Cancer and Prostate Cancer Early Detection. J Natl Compr Canc Netw (2018) 16: 620–623.
6. Miyake H, Sakai I, Inoue TA, Hara I and Fujisawa M: The limited significance of a longer duration of neoadjuvant hormonal therapy prior to radical prostatectomy for high-risk prostate cancer in Japanese men. Urol Int (2006) 77: 122–126.
7. Hassan O, Han M, Zhou A, Paulk A, Sun Y, Al-Harbi A, Alrajjal A, Baptista Dos Santos F and Epstein JI: Incidence of Extraprostatic

Extension at Radical Prostatectomy with Pure Gleason Score 3＋3＝6 (Grade Group 1) Cancer: Implications for Whether Gleason Score 6 Prostate Cancer Should be Renamed "Not Cancer" and for Selection Criteria for Active Surveillance. J Urol (2018) 199: 1482–1487.
8. Albers LF, Korving JC, van Elzakker EPM and Roshani H: Osteomyelitis of the Pubic Symphysis After Transrectal Biopsies of the Prostate. Urology (2018) 121: 29–32.
9. van der Leest M, Cornel E, Israël B, Hendriks R, Padhani AR, Hoogenboom M, Zamecnik P, Bakker D, Setiasti AY, Veltman J, van den Hout H, van der Lelij H, van Oort I, Klaver S, Debruyne F, Sedelaar M, Hannink G, Rovers M, Hulsbergen-van de Kaa C and Barentsz JO: Head-to-head Comparison of Transrectal Ultrasound-guided Prostate Biopsy Versus Multiparametric Prostate Resonance Imaging with Subsequent Magnetic Resonance-guided Biopsy in Biopsy-naïve Men with Elevated Prostate-specific Antigen: A Large Prospective Multicenter Clinical Study. Eur Urol (2019) 75: 570–578.
10. Borghesi M, Ahmed H, Nam R, Schaeffer E, Schiavina R, Taneja S, Weidner W and Loeb S: Complications After Systematic, Random, and Image-guided Prostate Biopsy. Eur Urol (2017) 71: 353–365.
11. Rajkomar A, Dean J and Kohane I: Machine Learning in Medicine. N Engl J Med (2019) 380: 1347–1358.
12. Cuocolo R, Cipullo MB, Stanzione A, Ugga L, Romeo V, Radice L, Brunetti A and Imbriaco M: Machine learning applications in prostate cancer magnetic resonance imaging. Eur Radiol Exp (2019) 3: 35.
13. Sun Y, Reynolds HM, Parameswaran B, Wraith D, Finnegan ME, Williams S and Haworth A: Multiparametric MRI and radiomics in prostate cancer: a review. Australas Phys Eng Sci Med (2019) 42: 3–25.
14. Schelb P, Kohl S, Radtke JP, Wiesenfarth M, Kickingereder P, Bickelhaupt S, Kuder TA, Stenzinger A, Hohenfellner M, Schlemmer HP, Maier-Hein KH and Bonekamp D: Classification of Cancer at Prostate MRI: Deep Learning versus Clinical PI-RADS Assessment. Radiology (2019) 293: 607–617.
15. Antonelli M, Johnston EW, Dikaios N, Cheung KK, Sidhu HS, Appayya MB, Giganti F, Simmons LAM, Freeman A, Allen C, Ahmed HU, Atkinson D, Ourselin S and Punwani S: Machine learning classifiers can predict Gleason pattern 4 prostate cancer with greater accuracy than experienced radiologists. Eur Radiol (2019) 29: 4754–4764.
16. Bleker J, Kwee TC, Dierckx RAJO, de Jong IJ, Huisman H and Yakar D: Multiparametric MRI and auto-fixed volume of interest-based radiomics signature for clinically significant peripheral zone prostate cancer. Eur Radiol (2020) 30: 1313–1324.
17. Bagher-Ebadian H, Janic B, Liu C, Pantelic M, Hearshen D, Elshaikh M, Movsas B, Chetty IJ and Wen N: Detection of Dominant Intra-prostatic Lesions in Patients With Prostate Cancer Using an Artificial Neural Network and MR Multi-modal Radiomics Analysis. Front Oncol (2019) 9: 1313.
18. Chaddad A, Kucharczyk M and Niazi T: Multimodal radiomic features for the predicting gleason score of prostate cancer. Cancers (Basel) (2018) 10: 249.
19. Monti S, Brancato V, Costanzo GD, Basso L, Puglia M, Ragozzino A, Salvatore M and Cavaliere C: Multiparametric MRI for prostate cancer detection: New insights into the combined use of a radiomic approach with advanced acquisition protocol. Cancers (2020) 12: 390.
20. Turkbey B, Rosenkrantz AB, Haider MA, Padhani AR, Villeirs G, Macura KJ, Tempany CM, Choyke PL, Cornud F, Margolis DJ, Thoeny HC, Verma S, Barentsz J and Weinreb JC: Prostate Imaging Reporting and Data System Version 2.1: 2019 Update of Prostate Imaging Reporting and Data System Version 2. Eur Urol (2019) 76: 340–351.
21. Demšar J, Curk T, Erjavec A, Gorup Č, Hočevar T, Milutinovič M, Možina M, Polajnar M, Toplak M, Starič A and Štajdohar M: Orange: data mining toolbox in Python. J Mach Learn Res (2013) 14: 2349–2353.
22. Tilki D, van den Bergh RCN, Briers E, Van den Broeck T, Brunckhorst O, Darraugh J, Eberli D, De Meerleer G, De Santis M, Farolfi A, Gandaglia G, Gillessen S, Grivas N, Henry AM, Lardas M, JLH van Leenders G, Liew M, Linares Espinos E, Oldenburg J, van Oort IM, Oprea-Lager DE, Ploussard G, Roberts MJ, Rouvière O, Schoots IG, Schouten N, Smith EJ, Stranne J, Wiegel T, Willemse PM and Cornford P: EAU-EANM-ESTRO-ESUR-ISUP-SIOG Guidelines on Prostate Cancer-2024 Update. Part I: Screening, Diagnosis, and Local Treatment with Curative Intent. Eur Urol (2024) 29: 02306–6.
23. Khalvati F, Wong A and Haider MA: Automated prostate cancer detection via comprehensive multi-parametric magnetic resonance imaging texture feature models. BMC Med Imaging (2015) 15: 27.
24. Kwak JT, Xu S, Wood BJ, Turkbey B, Choyke PL, Pinto PA, Wang S and Summers RM: Automated prostate cancer detection using T2-weighted and high-b-value diffusion-weighted magnetic resonance imaging. Med Phys (2015) 42: 2368–2378.
25. Zhao C, Gao G, Fang D, Li F, Yang X, Wang H, He Q and Wang X: The efficiency of multiparametric magnetic resonance imaging (mpMRI) using PI-RADS Version 2 in the diagnosis of clinically significant prostate cancer. Clin Imaging (2016) 40: 885–888.
26. Chen T, Li M, Gu Y, Zhang Y, Yang S, Wei C, Wu J, Li X, Zhao W and Shen J: Prostate Cancer Differentiation and Aggressiveness: Assessment With a Radiomic-Based Model vs. PI-RADS v2. J Magn Reson Imaging (2019) 49: 875–884.
27. Hegde JV, Mulkern RV, Panych LP, Fennessy FM, Fedorov A, Maier SE and Tempany CM: Multiparametric MRI of prostate cancer: an update on state-of-the-art techniques and their performance in detecting and localizing prostate cancer. J Magn Reson Imaging (2013) 37: 1035–1054.
28. Donati OF, Mazaheri Y, Afaq A, Vargas HA, Zheng J, Moskowitz CS, Hricak H and Akin O: Prostate cancer aggressiveness: assessment with whole-lesion histogram analysis of the apparent diffusion coefficient. Radiology (2014) 271: 143–152.
29. Chen T, Zhang Z, Tan S, Zhang Y, Wei C, Wang S, Zhao W, Qian X, Zhou Z, Shen J, Dai Y and Hu J: MRI Based Radiomics Compared With the PI-RADS V2.1 in the Prediction of Clinically Significant Prostate Cancer: Biparametric vs Multiparametric MRI. Front Oncol (2022) 11: 792456.
30. Zhang L, Zhe X, Tang M, Zhang J, Ren J, Zhang X and Li L: Predicting the Grade of Prostate Cancer Based on a Biparametric MRI Radiomics Signature. Contrast Media Mol Imaging (2021) 2021: 7830909.
31. Bagher-Ebadian H, Janic B, Liu C, Pantelic M, Hearshen D, Elshaikh M, Movsas B, Chetty IJ and Wen N: Detection of Dominant Intra-prostatic Lesions in Patients With Prostate Cancer Using an Artificial Neural Network and MR Multi-modal Radiomics Analysis. Front Oncol (2019) 9: 1313.
32. van Griethuysen JJM, Fedorov A, Parmar C, Hosny A, Aucoin N, Narayan V, Beets-Tan RGH, Fillion-Robin JC, Pieper S and Aerts HJWL: Computational Radiomics System to Decode the Radiographic Phenotype. Cancer Res (2017) 77: e104–e107.